

# Dzyaloshinskii-Moriya interaction chirality reversal with ferromagnetic thickness

Capucine Gueneau<sup>¶</sup>, Fatima Ibrahim<sup>¶</sup>, Johanna Fischer<sup>1\*</sup>, Libor Vojáček<sup>1</sup>, Charles-Élie Fillion<sup>1</sup>, Stefania Pizzini<sup>2</sup>, Laurent Ranno<sup>2</sup>, Isabelle Joumard<sup>1</sup>, Stéphane Auffret<sup>1</sup>, Jérôme Faure-Vincent<sup>1</sup>, Claire Baraduc<sup>1</sup>, Mairbek Chshiev<sup>1,3</sup>, and Hélène Béa<sup>1,3\*</sup>

<sup>1</sup>Univ. Grenoble Alpes, CEA, CNRS, Spintec, 38000 Grenoble, France

<sup>2</sup>Univ. Grenoble Alpes, CNRS, Néel Institute, 38042 Grenoble, France

<sup>3</sup>Institut Universitaire de France (IUF), 75000 Paris, France

¶ C.G. and F.I. contributed equally

\* Corresponding authors, Johanna.fischer@cea.fr, Helene.bea@cea.fr

## ABSTRACT.

In ultrathin ferromagnetic films sandwiched between two distinct heavy metal layers or between a heavy metal and an oxide layer, the Dzyaloshinskii-Moriya interaction (DMI) is recognized as being of interfacial origin. Its chirality and strength are determined by the properties of the adjacent heavy metals and the degree of oxidation at the interfaces. Here, we demonstrate that the chirality of the DMI can change solely with variations in the thickness of the ferromagnetic layer - an effect that has not been experimentally observed or explained until now. Our experimental observation in the trilayer system Ta/FeCoB/TaOx is supported by *ab initio* calculations: they reveal that variations in orbital filling and inter-atomic distances at the interface, driven by the number of ferromagnetic atomic layers, lead to an inversion of DMI chirality. This mechanism takes place for ferromagnetic layers with more than three atomic layers, for which the two interfaces start to be decoupled. We hence propose a new degree of freedom to tune DMI chirality and the associated chiral spin textures by tailoring crystal structure e.g. using strain or surface acoustic waves.

## I. INTRODUCTION

The Dzyaloshinskii-Moriya interaction (DMI) is an antisymmetric exchange interaction that can stabilize chiral spin textures or a cycloidal order. Recent experiments focused on ultrathin multilayers with perpendicular magnetic anisotropy (PMA), where spin textures such as skyrmions or chiral domain walls are stabilized at room temperature [1], and efficiently moved by the injection of an electric current via spin-orbit torques [2,3]. Ultrathin heavy metal/ferromagnet/oxide (HM/FM/MOx) trilayers with PMA [4,5] offer a promising platform to study interfacial DMI which arises from the combination of spin-orbit coupling and structural inversion asymmetry at the two FM interfaces [6,7]. Specifically, the antisymmetric exchange between neighboring spins is mediated by the conduction electrons, which experience either spin-orbit interaction within the HM layer (Fert-Levy mechanism) [8] or a Rashba field at the FM/MOx interface (Rashba-type DMI) [9]. The interfacial DMI arises at both interfaces with a strength and chirality quantified by a coefficient  $D$  depending on the nature of the HM and on the oxidation state of the oxide layer. It imposes a given domain wall type and chirality and is usually considered to be the sum of the

contributions from the top and bottom interfaces. The interfacial character can be modeled by  $D = \frac{D_s}{t}$ . Here,  $t$  denotes the thickness of the ferromagnet, and  $D_s$  the interfacial DMI coefficient comprising both interface contributions. The material-dependence of DMI in heavy-metal/ferromagnet systems has been demonstrated experimentally in [10–13] and analyzed theoretically in [14,15]. Furthermore, tuning the DMI chirality with the oxidation of the FM/MOx interfaces has been predicted [16,17] and observed in similar trilayer structures [18]. However, the dependence of the DMI chirality solely on the ferromagnetic thickness without a variation in oxidation state has neither been systematically studied nor theoretically predicted.

## II. RESULTS

In this Letter, we present the DMI chirality inversion with ferromagnetic thickness, supported by both theoretical modeling (Fig. 1(a)) and experimental validation (Fig. 1(b)), to investigate the interfacial DMI in a weak DMI system, namely Ta/FeCoB/TaOx. Designing perpendicular wedges of the ferromagnetic and top metal layers enables gradual variation of ferromagnet thickness independent of the FM/oxide interface oxidation gradient. This crossed double wedge method, unlike that in [18], differentiates interfacial effects from ferromagnetic thickness-related DMI changes, providing deeper insight into their respective contributions. The DMI chirality is unambiguously determined from the current-driven direction of motion of domain walls (DWs) and skyrmions [19]. This motion results from spin-orbit torque, with direction depending on clockwise (CW) or counter-clockwise (CCW) spin structure chirality (Fig. 1). To elucidate the underlying mechanisms of the observed DMI chirality changes, we performed *ab initio* calculations. The agreement between experiment and theory on the DMI sign variation with both the ferromagnet thickness and oxidation state enables to untangle the mechanisms governing the DMI chirality. In particular, the DMI sign inversion with increasing the number of FM monolayers arises from changes in electronic orbital filling due to modified inter-layer distance ( $z$ ) between the FM and HM layers (Fig. 1(b)). This study paves the way to deterministic control of skyrmions and chiral domain walls by tuning the ferromagnetic thickness.

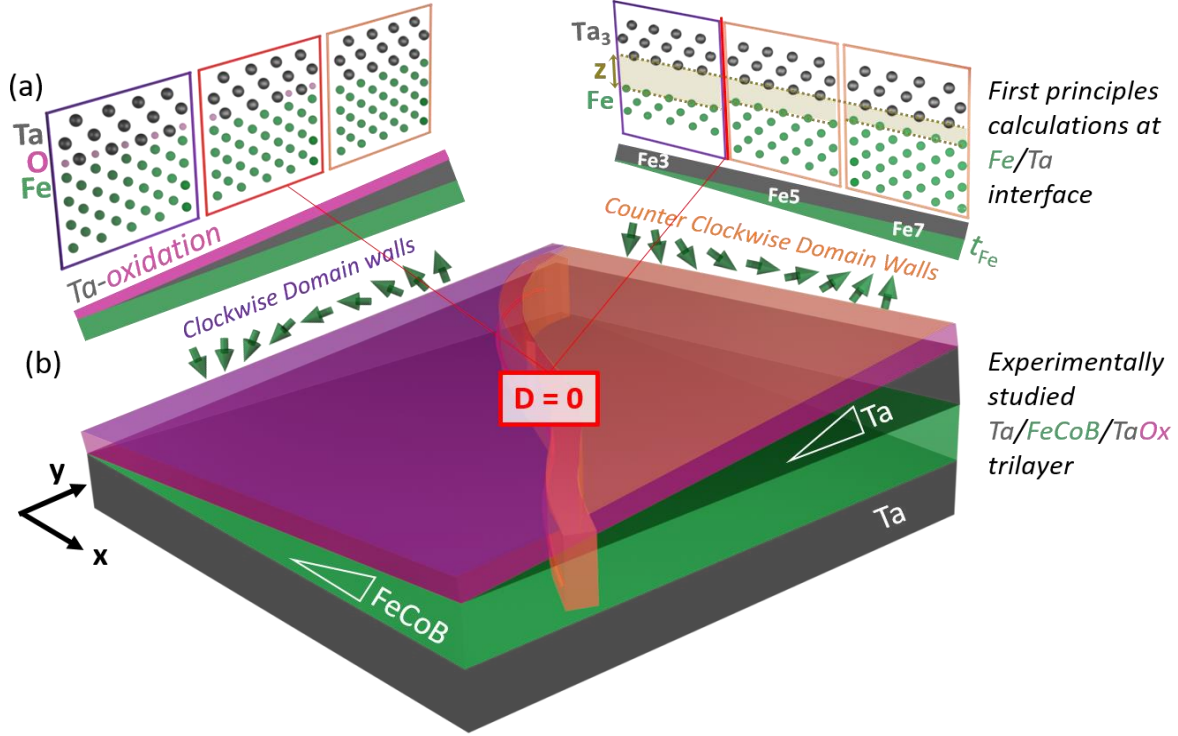


Fig. 1 Combination of the experimentally studied (Ta/FeCoB/TaOx) double wedge trilayer system (b) with the theoretically analyzed Fe/Ta(Ox) top interface (a). In the schematic illustration (b) the red band represents the DMI sign change ( $D = 0$ ) with increasing ferromagnet thickness along  $x$  and decreasing degree of oxidation of the top heavy metal layer along  $y$  and domain walls with the respective chirality (CW/CCW) in the violet/orange zone left/right of  $D=0$ . A projection (a) of the associated crystallographic structure at the top interface, used for the ab-initio calculations, is depicted along each wedge; green/gray/purple balls represent Fe/Ta/O atoms.  $z$  is the relaxed Fe-Ta plane distance.

## A. Experimental results

The studied system is a sputtered Ta/FeCoB/TaOx trilayer with weak DMI strength ( $< \text{hundreds of } \mu\text{J}/\text{m}^2$ ). A homogeneous bottom Ta/FeCoB interface is achieved by depositing the Ta layer at constant thickness, while crossed wedges of FeCoB and top Ta layers create gradients: FeCoB thickness varies along the  $x$ -axis while the oxidation state of TaOx along the  $y$ -axis since the top Ta is oxidized after deposition (Fig. 1(b) and APPENDIX A). Hence, for a given ferromagnet thicknesses, we obtain different oxidation states at the top interface: under-oxidized (FeCoB/Ta(Ox)), optimally oxidized associated to maximum PMA (FeCoB/TaOx), and over-oxidized (FeCoBOx/TaOx) regions. Conversely, for a fixed oxidation state, the ferromagnet thickness varies continuously. We first discuss the effect of ferromagnetic thickness ( $t$ ) and the degree of oxidation at the FeCoB/TaOx interface on the magnetic anisotropy. The effective anisotropy,  $K_{eff} = \frac{K_s}{t} - K_d$ , depends on the surface  $K_s$  and the dipolar  $K_d = \frac{1}{2} \mu_0 M_s^2$  anisotropy constants. Variations in  $t$  directly influence  $K_{eff}$ , while changes in oxidation state impacts interfacial properties, specifically  $K_s$ .

At a critical thickness  $t_c$  of the ferromagnet,  $K_d$  overcomes the surface contribution  $\frac{K_s}{t}$ , leading to a change in sign of  $K_{eff}$  which corresponds to the crossover between PMA and In-Plane (IP) anisotropy. For ultrathin ferromagnet, size effects and dead layers induce a paramagnetic (PM) regime at room temperature [20,21].

Magnetometry measurements using the polar magneto-optic Kerr effect (p-MOKE) reveal square hysteresis loops in PMA regions (dark grey, Fig. 2(a)) and remanence loss in surrounding intermediate grey regions. This loss arises from labyrinthine or stripe domain formation at zero magnetic field due to reduced  $K_{eff}$ . As  $t$  increases, the system transitions into the IP anisotropy region (light grey in

Fig. 2(a)), where  $K_{eff}$  changes sign. The proximity of remanence loss and  $K_{eff}$  transition regions highlights remanence as a reliable indicator of anisotropy changes. Now starting from PMA region and decreasing  $t$ , leads to a PM region with  $K_{eff}$  and saturation magnetization dropping to zero, also inducing remanence loss.

Both wedges in the system induce anisotropy transitions, with the PMA-to-IP transition occurring at a FeCoB thickness of approximately 1.1–1.2 nm. Additionally, for top Ta thinner than 0.9 nm, the PMA region narrows with decreasing thickness. This indicates partial oxidation of FeCoB, creating a FeCoB/FeCoBO<sub>x</sub>/TaO<sub>x</sub> top interface. On the other hand, for Ta > 1 nm, increasing Ta thickness reduces the PMA region, leading to a PM regime. The resulting underoxidized FeCoB/Ta/TaO<sub>x</sub> interface causes a loss of magnetism due to the decrease of magnetic order induced by Fe/Ta orbital hybridization [22]: our *ab initio* calculations find a 20% reduction of the magnetic moment of the Fe atom at the Ta interface (Supplementary 1). The interfacial disorder in experimental samples may also reduce ferromagnetic order.

In the low remanence regions showing demagnetized state at zero magnetic field, the application of a small perpendicular magnetic field (< 1 mT) allows to nucleate skyrmions. Brillouin Light Scattering (BLS) measurements demonstrated a sign inversion of the DMI with the oxidation of the FeCoB/TaO<sub>x</sub> interface (red star and cross in

Fig. 2(a)) [23], resulting in the emergence of skyrmions with both chiralities. To better understand the DMI behavior and its dependence on the FeCoB/TaO<sub>x</sub> interface oxidation state and FeCoB layer thickness, we map the chirality of the spin textures. We measure the sign of a small DMI amplitude in a large number of wafer positions (undoable with BLS measurements) from the direction of the current-induced motion of DWs, observed with polar MOKE microscopy. This technique is based on spin-orbit torque (SOT) and implies that the direction of motion depends on the chirality of the magnetic texture: CW (resp. CCW) DW moves along (resp. opposite to) the current direction when using a HM with a negative spin Hall angle like Ta [19].

In

Fig. 2(a), we present a systematic study of the influence of FeCoB thickness and FeCoB/TaO<sub>x</sub> oxidation state on DMI chirality over the whole PMA region (see examples of MOKE images in

Fig. 2(b)). Each square indicates a current application point where DW motion is analyzed to determine the chirality and the DMI sign. The regions exhibiting CCW and CW chirality are depicted in orange and purple, respectively. The red zero DMI line indicates the DMI chirality transition, for which nearly no motion of domain walls is visible. This line joins the red cross and star previously observed in the skyrmion region [23]. For a fixed FeCoB thickness (vertical line in Fig. 2(a)), DMI chirality changes with top Ta thickness and oxidation state, which is consistent with [16,18].

Surprisingly, we observe a DMI chirality inversion for a fixed top Ta thickness when varying FeCoB thickness (horizontal line in

Fig. 2(a)). This unexpected dependence of DMI chirality on FeCoB thickness is evident across several FeCoB/TaOx oxidation states. The effective DMI in our sample can be considered as the sum of contributions from both interfaces [24,25]. The sign of the DMI contribution from the top FM/oxide interface was shown to be dependent on oxidation [16,18,30]. The DMI contribution from the bottom Ta/FeCoB interface is usually around  $D = 20 - 30 \mu\text{J}/\text{m}^2$  [23] which corresponds to  $D_s = 20 - 30 \text{ fJ}/\text{m}$  [27,28]. BLS measurements in low remanence regions revealed DMI values around  $D = -100 \mu\text{J}/\text{m}^2$  near the PM/PMA transition (slightly thinner top Ta than the red cross in Fig. 2(a)) [29] and  $\pm 100 \mu\text{J}/\text{m}^2$  near the PMA/IP transition for top Ta thicker (thinner) than the red star, respectively [23,30]. For these three measurements, removing the bottom interface contribution showed that the top FeCoB/TaOx DMI contribution changes sign [23]. Hence, the sign of the surface DMI,  $D_s$ , originating from the top FM/MOx interface, depends on the oxidation degree. Remarkably, the sign of  $D_s$ , also changes with the FM thickness, a result that has not yet been unambiguously reported experimentally.

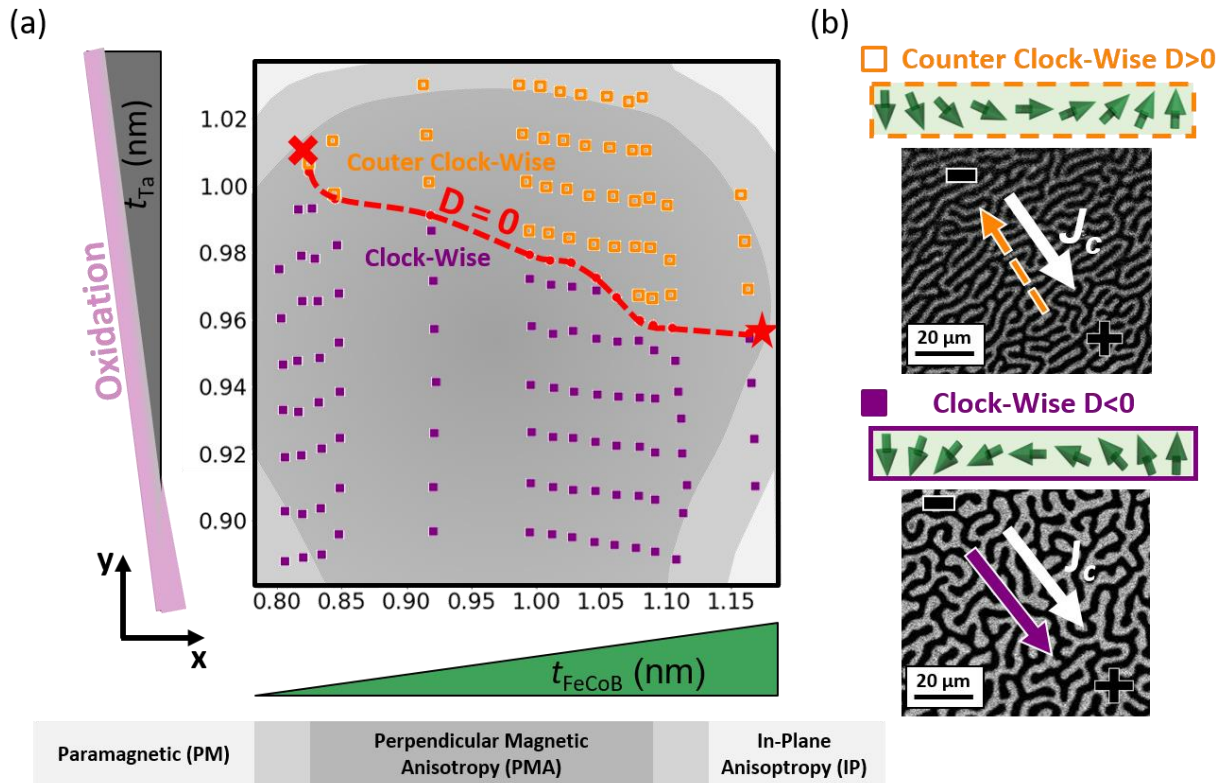


Fig. 2 (a) Map of the DW chirality in the PMA region (dark grey) with respect to FeCoB thickness ( $t_{\text{FeCoB}}$ ) and oxidation state ( $t_{\text{Ta}}$ ). At the border of PMA region (intermediate grey), spontaneous demagnetization occurs at zero magnetic field, creating domains and DWs. Measured points with CW (resp. CCW) DWs are represented with full purple squares (resp. empty orange squares). Red dashed line represents DMI sign crossover and corresponds to no DW motion. It meets the DMI sign inversion observed in skyrmion regions (red star and cross) [23]. (b) Differential

*MOKE images are shown for both domain wall chiralities. The current direction  $J_c$  and the DW motion are represented by a white and orange/purple arrow respectively.*

## **B. *Ab-initio* calculations**

To understand the observed DMI sign inversion with the FM thickness, we conducted *ab-initio* calculations.  $\text{Fe}_n/\text{Ta}_m$  bilayer with variable Fe thickness and Ta oxidation state,  $n$  and  $m$  representing the number of monolayers MLs (Fig. 1a), is used to model the top interface of our sample, FeCoB/TaOx. The calculated DMI energy  $E_{DMI}$  is proportional to the interfacial DMI coefficient  $D_s$ . Fig. 3a summarizes the variation of  $E_{DMI}$  as a function of both the Fe thickness (3-9 MLs) and the oxidation percentage (0-100%) of the interfacial Ta layer where different effects can be distinguished. First,  $E_{DMI}$  is highly dependent on the Ta oxidation percentage for all Fe thicknesses. Notably, for 5 to 9 Fe MLs, the DMI changes sign at low oxidation percentages below 25% beyond which its value increases. This DMI sign change with Ta oxidation is consistent with the experimental map in

Fig. 2. Indeed, *ab initio* calculations deal with single crystalline structures, whereas our experimental samples are polycrystalline, which might explain an offset in transition thickness values. Noteworthy, oxidizing the interfacial Ta layer is sufficient to model the TaOx in the experimental sample (supplementary 5).

Importantly, a DMI sign change between three and five Fe monolayers is found for the unoxidized interface. This is qualitatively consistent with our experimental observation of DMI sign change for increased FM layer thickness at small and constant FeCoB/TaOx oxidation state (upper part of the map in

Fig. 2(b)). A quantitative comparison remains difficult since the experimental effective DMI includes the small contribution from the bottom Ta/FeCoB, independent on the FeCoB or Ta top thicknesses [23]. For higher percentages of Ta oxidation, no DMI sign change with Fe thickness is found, which consistently corresponds to intermediate thicknesses of the top Ta layer (below 0.95 nm) in the experimental sample. Finally, the simultaneous oxidation of interfacial Ta and Fe (Fig. 3d) tends to decrease the DMI values and a further decrease occurs for thicker Fe layers. This shall correspond to thinner Ta regions than studied in Fig. 2. The small DMI predicted in this overoxidized region is interesting for a potential reversal of the chirality by applying a gate voltage [30], but is beyond the scope of the present study.

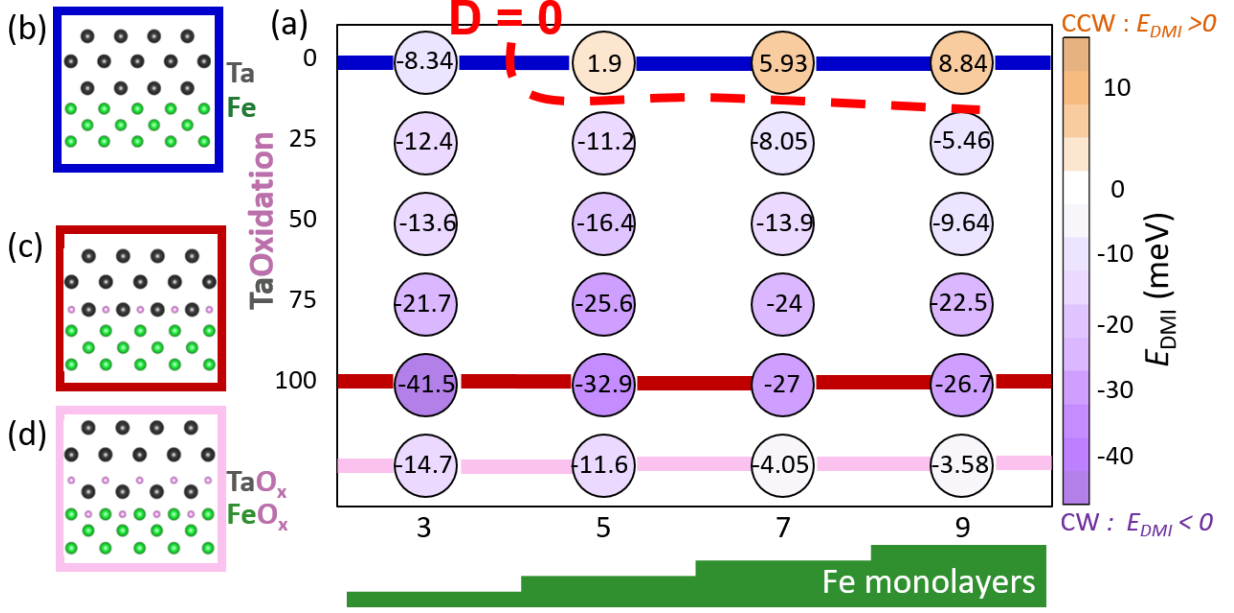


Fig. 3 Theoretical DMI map. (a) DMI energy ( $E_{DMI}$ ) calculated for varied Ta oxidation state (in percentage) and Fe thickness (in monolayers) in Ta/Fe interface. The crystallographic structures used are shown for (b) non-oxidized Ta, (c) fully oxidized Ta, and (d) simultaneously oxidized Ta and Fe interface. The red dashed line designates the DMI sign inversion.

As the oxidation effect on the DMI has been studied before [16–18,31], we focus here on the mechanism underlying the dependence of the DMI on the FM thickness at the Fe/Ta interface. Due to the interfacial character of  $D_S$ , it is unexpected that its sign may depend on the FM thickness. Fig. 4a presents the layer-resolved difference in the chirality-dependent spin-orbit coupling (SOC) energy i.e.  $\Delta E_{soc}^k = E_{cw}^k - E_{ccw}^k$  where  $k$  is the atomic layer. As expected from the Fert-Levy DMI mechanism [8], the SOC energy is predominantly located at the interfacial Ta1 layer. Interestingly, it shows a remarkable sign crossover between  $Ta_3Fe_3$  and  $Ta_3Fe_5$  structures, which is at the origin of the overall DMI sign change. Noteworthy, the Ta2 and Ta3 layers hold minor and cancelling contributions to the overall spin-orbit energy which justifies the choice of a three-monolayer thick Ta layer in our calculations (Supplementary 4).

Of note, the Fe/vacuum interface has a non-negligible contribution to  $E_{DMI}$ . For  $Ta_3Fe_5$ ,  $Ta_3Fe_7$  and  $Ta_3Fe_9$  in Fig. 4a, the three Fe atoms close to vacuum have a similar contribution to SOC energy. However, for the ultra-thin  $Ta_3Fe_3$ , a vacuum contribution cannot be disentangled from the Fe/Ta interface contribution, which makes this correction difficult to perform. Overall, the vacuum interface contribution to the total  $E_{DMI}$  might shift a bit the Fe thickness at which the DMI changes sign. Nevertheless, the proposed mechanism of the inversion of the Ta1 SOC energy mainly contributing to the DMI sign inversion, remains valid.

A microscopic insight into the DMI dependence on the FM thickness is acquired by comparing the variation of  $5d$  orbital-resolved SOC energy of interfacial Ta1 layer in  $Ta_3Fe_3$  and  $Ta_3Fe_5$  (Fig. 4(b, c)). A substantial difference is observed in the SOC matrix element contribution corresponding to the hybridization between  $d_{z^2}$  and  $d_{xz}$  orbitals, which is strongly negative for  $Ta_3Fe_3$  and becomes positive by increasing the Fe thickness in  $Ta_3Fe_5$ .

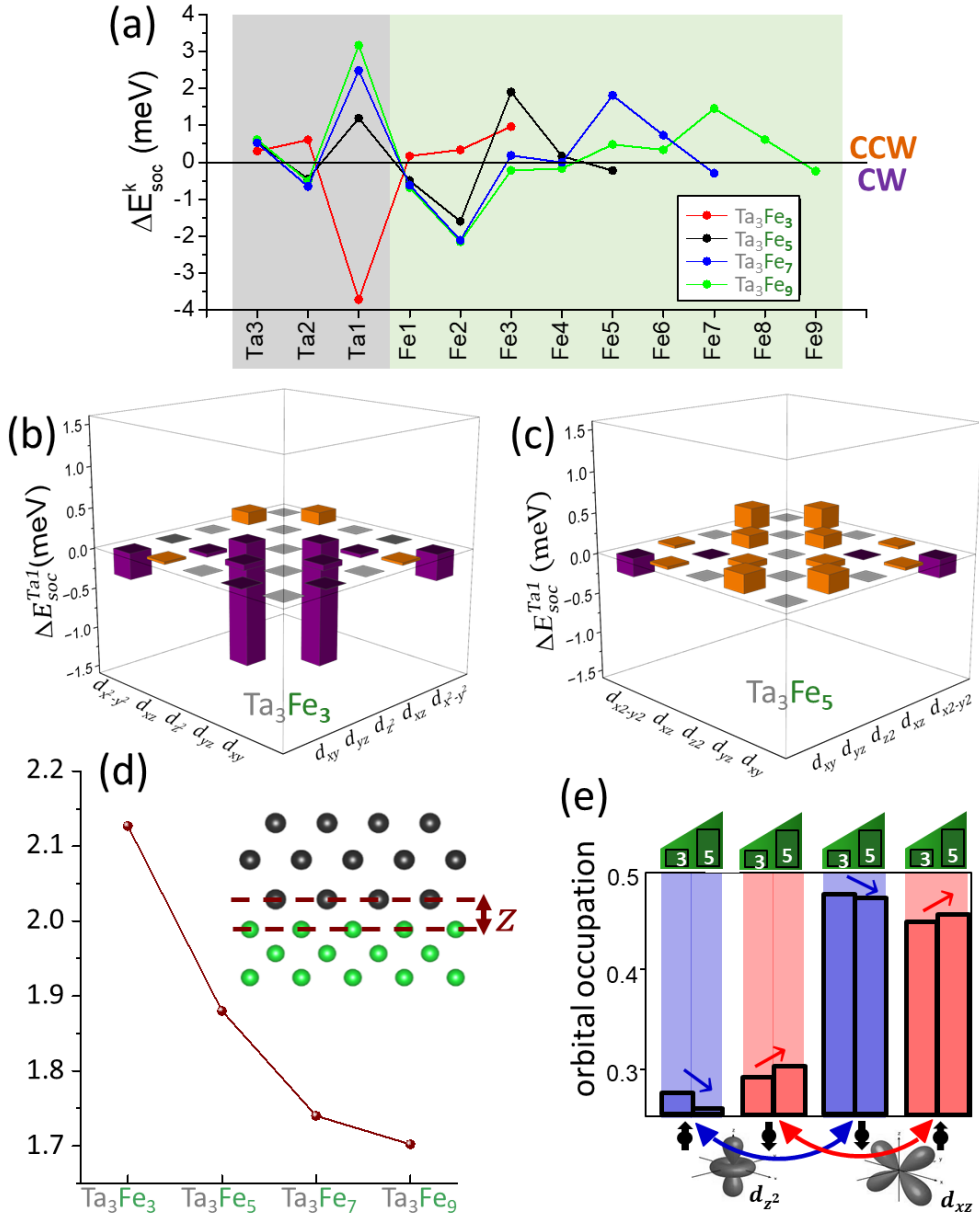


Fig. 4 Mechanism of the DMI dependence on the FM thickness. (a) Layer resolved difference in the chirality-dependent spin-orbit coupling energy  $\Delta E_{soc}^k$  calculated for Ta/Fe structures with variable Fe thickness. Variation of 5d orbital-resolved SOC energy of interfacial Ta1 layer in (b)  $Ta_3Fe_3$  and (c)  $Ta_3Fe_5$ . (d) Variation of the interfacial distance 'z' between Ta1-Fe1 (inset) for the different calculated structures. (e) The spin dependent d-orbital occupations (precisely  $d_{z^2}$  and  $d_{xz}$ ) of Ta1 in  $Ta_3Fe_3$  and  $Ta_3Fe_5$ , referred to as 3 and 5.

In the framework of the first-order perturbation theory [32,33], the occupied 5d orbital states of the interfacial Ta1 layer mainly contribute to the DMI. Consequently, the corrections to the total energy due to DMI can be approximated by the expectation value of the SOC operator as  $\langle \psi_{lm,s} | \hat{H}_{soc} | \psi_{lm,s} \rangle$  where  $|\psi_{lm,s}\rangle$  represents the spin-dependent



occupied states of Ta1. Considering the spin-mixing transition terms between fully-occupied  $d$ -orbitals, the highest contribution to DMI is given by the expectation value of the SOC matrix elements  $\langle d_{z^2}^\uparrow + d_{xz}^\downarrow | \hat{H}_{soc} | d_{z^2}^\uparrow + d_{xz}^\downarrow \rangle = -\sqrt{6}$  and  $\langle d_{z^2}^\downarrow + d_{xz}^\uparrow | \hat{H}_{soc} | d_{z^2}^\downarrow + d_{xz}^\uparrow \rangle = \sqrt{6}$  [33]. This is consistent with our finding from orbital-resolved SOC energies where  $d_{z^2}^\uparrow + d_{xz}^\downarrow$  contributes the largest change (Fig. 4(b,c)). However, to explain the sign change it is relevant to compare the  $d$ -orbital occupations of Ta1 in Ta<sub>3</sub>Fe<sub>3</sub> and Ta<sub>3</sub>Fe<sub>5</sub> shown in Fig. 4(e). On one hand, the decrease of both the  $d_{z^2}^\uparrow$  and  $d_{xz}^\downarrow$  occupation leads to a decrease in the  $\langle d_{z^2}^\uparrow + d_{xz}^\downarrow | \hat{H}_{soc} | d_{z^2}^\uparrow + d_{xz}^\downarrow \rangle$  matrix element when increasing the Fe thickness from three to five monolayers. At the same time, the increase of the  $d_{z^2}^\downarrow$  and  $d_{xz}^\uparrow$  occupation yields an increase in the  $\langle d_{z^2}^\downarrow + d_{xz}^\uparrow | \hat{H}_{soc} | d_{z^2}^\downarrow + d_{xz}^\uparrow \rangle$  matrix element. Simultaneously, these two effects add a positive contribution to the SOC energy of the interfacial Ta1 layer, which in turn dictates the overall CW to CCW DMI sign crossover with the increase in Fe thickness. A detailed calculation of the interlayer and intralayer contributions to DMI are presented in supplementary 3.

The change in the  $d$ -orbital occupation can be attributed to the structural relaxation upon increasing the FM thickness. In Fig. 4(d), as the Fe thickness increases, the interfacial distance  $z$  between Ta1-Fe1 decreases which triggers the change in the occupation of the overlapping  $d$ -orbitals, mainly the out-of-plane  $d_{z^2}$  and  $d_{xz}$ . This affects the DMI energy, as seen above, but also the PMA and the FM magnetic moment (Supplementary 1). We stress that this DMI sign change with FM thickness originates from spin-orbit coupling in the unoxidized top Ta heavy metal and is thus attributed to a Fert-Levy DMI mechanism. Recently a Rashba-type DMI sign change was predicted at the Fe/MgO interface with increasing Fe thicknesses from 1 to 5 monolayers [26]. The change of DMI sign with FM thickness in the ultrathin regime might thus occur in other systems, which would be interesting to explore experimentally.

### III. CONCLUSIONS

To summarize, we have conducted a combined experimental and *ab-initio* study in a heavy metal/ferromagnet/oxide trilayer with weak DMI. We have analyzed separately the influence of the oxidation state at the top FM/MOx interface and the FM thickness on the DMI chirality. Here, we unveil unprecedented dependence of the interfacial DMI chirality on the thickness of the FM layer. More precisely, for several MOx (M = Ta) oxidation states this leads to a variation of the effective DMI strength and even to its chirality inversion for an under-oxidized FM/M(Ox). Our *ab-initio* calculations reproduce our experimental findings and explain the origin of this effect by a variation of orbital filling induced by structural relaxation. This is directly linked to the strain in the material, thereby unlocking exciting opportunities for manipulating chiral domain walls and skyrmions through strain engineering. Timely, a novel research area is emerging where skyrmions may be nucleated and propagated using transient strain provided by surface acoustic waves [34–36].

### ACKNOWLEDGMENTS

The authors acknowledge funding by the French ANR (contracts ADMIS n°ANR-19-CE24-0019, CHIREX n°ANR-22-EXSP-0002). This project has received funding from the European Union’s Horizon 2020 research and innovation program under Grant Agreement No. 800945 (NUMERICS–H2020-MSCA-COFUND-2017).

## References

- [1] O. Boulle et al., Room-temperature chiral magnetic skyrmions in ultrathin magnetic nanostructures, *Nat. Nanotechnol.* **11**, 449 (2016).
- [2] S. Woo et al., Observation of room-temperature magnetic skyrmions and their current-driven dynamics in ultrathin metallic ferromagnets, *Nat. Mater.* **15**, 501 (2016).
- [3] W. Jiang et al., Blowing magnetic skyrmion bubbles, *Science* **349**, 283 (2015).
- [4] S. Peng et al., Origin of interfacial perpendicular magnetic anisotropy in MgO/CoFe/metallic capping layer structures, *Sci. Rep.* **5**, 18173 (2015).
- [5] A. Fert, N. Reyren, and V. Cros, Magnetic skyrmions: advances in physics and potential applications, *Nat. Rev. Mater.* **2**, 17031 (2017).
- [6] I. Dzyaloshinsky, A thermodynamic theory of “weak” ferromagnetism of antiferromagnetics, *J. Phys. Chem. Solids* **4**, 241 (1958).
- [7] T. Moriya, Anisotropic Superexchange Interaction and Weak Ferromagnetism, *Phys. Rev.* **120**, 91 (1960).
- [8] A. Fert and P. M. Levy, Role of Anisotropic Exchange Interactions in Determining the Properties of Spin-Glasses, *Phys. Rev. Lett.* **44**, 1538 (1980).
- [9] K.-W. Kim, H.-W. Lee, K.-J. Lee, and M. D. Stiles, Chirality from Interfacial Spin-Orbit Coupling Effects in Magnetic Bilayers, *Phys. Rev. Lett.* **111**, 216601 (2013).
- [10] X. Ma, G. Yu, C. Tang, X. Li, C. He, J. Shi, K. L. Wang, and X. Li, Interfacial Dzyaloshinskii-Moriya Interaction: Effect of 5 d Band Filling and Correlation with Spin Mixing Conductance, *Phys. Rev. Lett.* **120**, 157204 (2018).
- [11] X. Ma et al., Interfacial control of Dzyaloshinskii-Moriya interaction in heavy metal/ferromagnetic metal thin film heterostructures, *Phys. Rev. B* **94**, 180408 (2016).
- [12] J. Torrejon, J. Kim, J. Sinha, S. Mitani, M. Hayashi, M. Yamanouchi, and H. Ohno, Interface control of the magnetic chirality in CoFeB/MgO heterostructures with heavy-metal underlayers, *Nat. Commun.* **5**, 4655 (2014).
- [13] G. Chen et al., Large Dzyaloshinskii-Moriya interaction induced by chemisorbed oxygen on a ferromagnet surface, *Sci. Adv.* **6**, eaba4924 (2020).
- [14] V. Kashid, T. Schena, B. Zimmermann, Y. Mokrousov, S. Blügel, V. Shah, and H. G. Salunke, Dzyaloshinskii-Moriya interaction and chiral magnetism in 3 d – 5 d zigzag chains: Tight-binding model and *ab initio* calculations, *Phys. Rev. B* **90**, 054412 (2014).
- [15] H. Yang, O. Boulle, V. Cros, A. Fert, and M. Chshiev, Controlling Dzyaloshinskii-Moriya Interaction via Chirality Dependent Atomic-Layer Stacking, Insulator Capping and Electric Field, *Sci. Rep.* **8**, 12356 (2018).
- [16] A. Belabbes, G. Bihlmayer, S. Blügel, and A. Manchon, Oxygen-enabled control of Dzyaloshinskii-Moriya Interaction in ultra-thin magnetic films, *Sci. Rep.* **6**, 24634 (2016).
- [17] L. Wang, Y. Ga, Q. Cui, P. Li, J. Liang, Y. Zhou, S. Wang, and H. Yang, Oxidation engineered Dzyaloshinskii-Moriya interaction and topological magnetism at Fe/MgO bilayers, *Phys. Rev. B* **108**, 214404 (2023).
- [18] M. Arora, J. M. Shaw, and H. T. Nembach, Variation of sign and magnitude of the Dzyaloshinskii-Moriya interaction of a ferromagnet with an oxide interface, *Phys. Rev. B* **101**, 054421 (2020).
- [19] S. Emori, U. Bauer, S.-M. Ahn, E. Martinez, and G. S. D. Beach, Current-driven dynamics of chiral ferromagnetic domain walls, *Nat. Mater.* **12**, 611 (2013).
- [20] R. Jungblut, M. T. Johnson, J. aan de Stegge, A. Reinders, and F. J. A. den Broeder, Orientational and Structural Dependence of Magnetic Anisotropy of Cu/Ni/Cu Sandwiches: Misfit Interface Anisotropy, *J. Appl. Phys.* **75**, 6424 (1994).
- [21] M. T. Johnson, P. J. H. Bloemen, F. J. A. den Broeder, and J. J. de Vries, Magnetic Anisotropy in Metallic Multilayers, *Rep Prog Phys* **59**, 1409 (1996).
- [22] T. Srivastava, W. Lim, I. Joumard, S. Auffret, C. Baraduc, and H. Béa, Mapping different skyrmion phases in double wedges of Ta/FeCoB/TaOx trilayers, *Phys. Rev. B* **100**, 220401 (2019).
- [23] R. Kumar et al., Control of Skyrmion Chirality in Ta / Fe – Co – B / Ta O x Trilayers by Ta O x Oxidation and Fe – Co – B Thickness, *Phys. Rev. Appl.* **19**, 024064 (2023).
- [24] C. Moreau-Luchaire et al., Additive Interfacial Chiral Interaction in Multilayers for Stabilization of Small Individual Skyrmions at Room Temperature, *Nat. Nanotech* **11**, 444 (2016).
- [25] H. Yang, O. Boulle, V. Cros, A. Fert, and M. Chshiev, Controlling Dzyaloshinskii-Moriya Interaction via Chirality Dependent Atomic-Layer Stacking, Insulator Capping and Electric Field, *Sci. Rep.* **8**, 12356 (2018).

- [26] L. Wang, Y. Ga, Q. Cui, P. Li, J. Liang, Y. Zhou, S. Wang, and H. Yang, Oxidation engineered Dzyaloshinskii-Moriya interaction and topological magnetism at Fe/MgO bilayers, *Phys. Rev. B* **108**, 214404 (2023).
- [27] L. H. Diez et al., Enhancement of the Dzyaloshinskii-Moriya interaction and domain wall velocity through interface intermixing in Ta/CoFeB/MgO, *Phys. Rev. B* **99**, 054431 (2019).
- [28] X. Ma, G. Yu, C. Tang, X. Li, C. He, J. Shi, K. L. Wang, and X. Li, Interfacial Dzyaloshinskii-Moriya Interaction: Effect of  $d$  Band Filling and Correlation with Spin Mixing Conductance, *Phys Rev Lett* **120**, 157204 (2018).
- [29] T. Srivastava et al., Large-Voltage Tuning of Dzyaloshinskii–Moriya Interactions: A Route toward Dynamic Control of Skyrmion Chirality, *Nano Lett* **18**, 4871 (2018).
- [30] C.-E. Fillion et al., Gate-controlled skyrmion and domain wall chirality, *Nat. Commun.* **13**, 5257 (2022).
- [31] D. de S. Chaves, F. Ajejas, V. Křizáková, J. Vogel, and S. Pizzini, Oxidation dependence of the Dzyaloshinskii-Moriya interaction in Pt/Co/MOx trilayers ( $M = \text{Al}$  or  $\text{Gd}$ ), *Phys. Rev. B* (2019).
- [32] M. Heide, G. Bihlmayer, and S. Blügel, Describing Dzyaloshinskii–Moriya spirals from first principles, *Phys. B Condens. Matter* **404**, 2678 (2009).
- [33] B. Yang, Q. Cui, J. Liang, M. Chshiev, and H. Yang, Reversible control of Dzyaloshinskii-Moriya interaction at the graphene/Co interface via hydrogen absorption, *Phys. Rev. B* **101**, 014406 (2020).
- [34] R. Chen, C. Chen, L. Han, P. Liu, R. Su, W. Zhu, Y. Zhou, F. Pan, and C. Song, Ordered creation and motion of skyrmions with surface acoustic wave, *Nat. Commun.* **14**, 1 (2023).
- [35] Y. Yang et al., Acoustic-driven magnetic skyrmion motion, *Nat. Commun.* **15**, 1 (2024).
- [36] T. Yokouchi, S. Sugimoto, B. Rana, S. Seki, N. Ogawa, S. Kasai, and Y. Otani, Creation of magnetic skyrmions by surface acoustic waves, *Nat. Nanotechnol.* **15**, 5 (2020).
- [37] P. E. Blöchl, Projector augmented-wave method, *Phys. Rev. B* **50**, 17953 (1994).
- [38] G. Kresse and J. Hafner, Ab initio molecular dynamics for liquid metals, *Phys. Rev. B* **47**, 558 (1993).
- [39] G. Kresse and J. Furthmüller, Efficient iterative schemes for ab initio total-energy calculations using a plane-wave basis set, *Phys. Rev. B* **54**, 11169 (1996).
- [40] G. Kresse and J. Furthmüller, Efficiency of ab-initio total energy calculations for metals and semiconductors using a plane-wave basis set, *Comput. Mater. Sci.* **6**, 15 (1996).
- [41] J. P. Perdew, K. Burke, and M. Ernzerhof, Generalized Gradient Approximation Made Simple, *Phys. Rev. Lett.* **77**, 3865 (1996).
- [42] H. Yang, A. Thiaville, S. Rohart, A. Fert, and M. Chshiev, Anatomy of Dzyaloshinskii-Moriya Interaction at Co / Pt Interfaces, *Phys. Rev. Lett.* **115**, 267210 (2015).

## APPENDIX A: Sample preparation

The sample was grown using on-axis and off-axis magnetron sputtering on a Si/SiO<sub>2</sub> 100 mm-diameter substrate. On-axis sputtering was employed to achieve uniform deposition, specifically for the bottom Ta layer. The target and the substrate are parallel and coaxial. A variation of 2 to 5 % thickness can be observed on the edge of the sample. We use off-axis deposition technique translating the sample with respect to the target, both remaining parallel, resulting in non-uniform thickness along one axis of the sample. This technique was employed to obtain the two gradient layers. We varied the deposition axis for each layer in order to have one gradient perpendicular to the other. The FeCoB target composition is Fe<sub>72</sub>Co<sub>8</sub>B<sub>20</sub>. We take the convention that the FeCoB thickness varies along the x-axis meanwhile the top Ta thickness is along the y-axis. The top Ta layer is oxidized naturally by exposition to oxygen in a treatment chamber. This leads to different oxidation states at the top interface named under-oxidized (FeCoB/Ta/TaO<sub>x</sub>), optimally oxidized (FeCoB/TaO<sub>x</sub>), and over-oxidized (FeCoBO<sub>x</sub>/TaO<sub>x</sub>). To protect the sample from extra oxidation and maintain its magnetic properties over time, a capping layer of 0.5 nm of Al is deposited in-situ. An annealing step is performed afterwards under vacuum at 225°C for 30min it increases the interface quality and enlarges the PMA region.

## APPENDIX B: Ab-initio calculations

Our first-principles calculations are based on the projector-augmented wave (PAW) method [37] as implemented in the VASP package [38–40] using the generalized gradient approximation [41] and including spin-orbit coupling. The Ta/Fe interface is modelled by a supercell of three monolayers Ta on top of Fe with varied thickness from three to nine monolayers followed by a sufficient vacuum layer of 20 Å. A pure Fe layer is considered since our FeCoB target composition is Fe rich (Fe<sub>72</sub>Co<sub>8</sub>B<sub>20</sub>) and boron migrates away from the ferromagnetic layer during annealing. The TaO<sub>x</sub> is modelled by adding oxygen atoms at the Ta interfacial layer with different Ta to O ratio to simulate varied oxidation percentages. The atomic coordinates are relaxed in the out-of-plane direction, with the in-plane parameter fixed to the bulk Fe, until the forces became smaller than 1 meV/Å. The DMI is calculated employing the constrained spin-spiral supercell method [42]. In this case, the DMI energy  $E_{DMI}$  is defined as the energy difference of the clockwise (CW) and counterclockwise (CCW) spin configurations where  $E_{DMI} = E_{CW} - E_{CCW}$ . Fig. 5 demonstrates the corresponding supercell structures with spin spirals rotating in the (*xz*)-plane. Note that in this convention, a positive (negative)  $E_{DMI}$  corresponds to a CCW (CW) DMI, respectively. The energy convergence criterium is set to  $10^{-7}$  eV to ensure a good convergence of the DMI energies. A kinetic energy cutoff of 500 eV has been used for the plane-wave basis set and a  $\Gamma$ -centered  $25 \times 25 \times 1$  k-mesh to sample the first Brillouin zone while a  $6 \times 24 \times 1$  mesh is used for the DMI calculations.

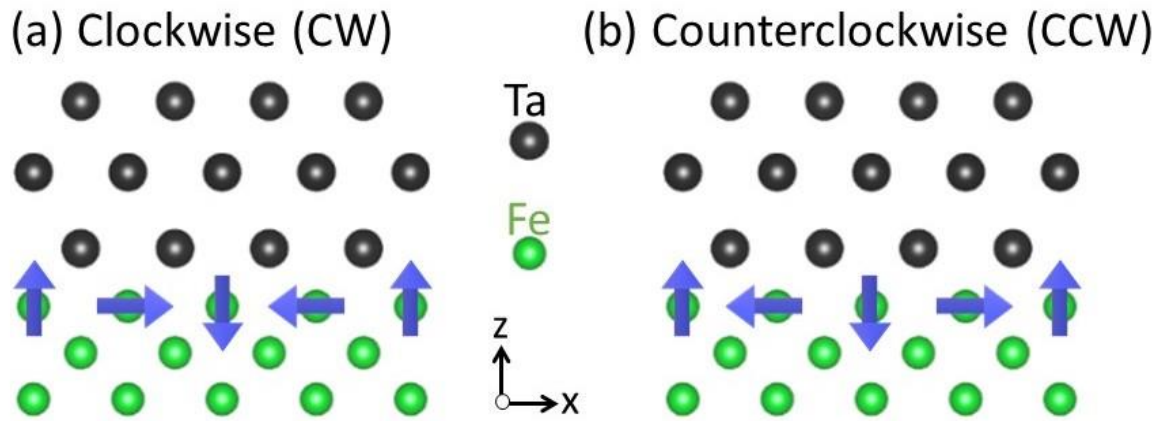


*Fig. 5 Ta/Fe supercell structures with spin spirals rotating in the  $(xz)$ -plane used to simulate (a) CW and (b) CCW configurations. The DMI energy is calculated as the difference in the total energy for those configurations. For clarity, the spins are shown only for one Fe layer.*

# Dzyaloshinskii-Moriya interaction chirality reversal with ferromagnetic thickness

Capucine Gueneau<sup>¶1</sup>, Fatima Ibrahim<sup>¶1</sup>, Johanna Fischer<sup>1\*</sup>, Libor Vojáček<sup>1</sup>, Charles-Élie Fillion<sup>1</sup>, Stefania Pizzini<sup>2</sup>, Laurent Ranno<sup>2</sup>, Isabelle Joumard<sup>1</sup>, Stéphane Auffret<sup>1</sup>, Jérôme Faure-Vincent<sup>1</sup>, Claire Baraduc<sup>1</sup>, Mairbek Chshiev<sup>1,3</sup>, and Hélène Béa<sup>1,3\*</sup>

<sup>1</sup>Univ. Grenoble Alpes, CEA, CNRS, Spintec, 38000 Grenoble, France

<sup>2</sup>Univ. Grenoble Alpes, CNRS, Néel Institute, 38042 Grenoble, France

<sup>3</sup>Institut Universitaire de France (IUF), 75000 Paris, France

<sup>¶</sup> C.G. and F.I. contributed equally

\* Corresponding authors, Johanna.fischer@cea.fr, Helene.bea@cea.fr

## Supplementary Material:

### 1. Magnetic moments in Ta/Fe interface

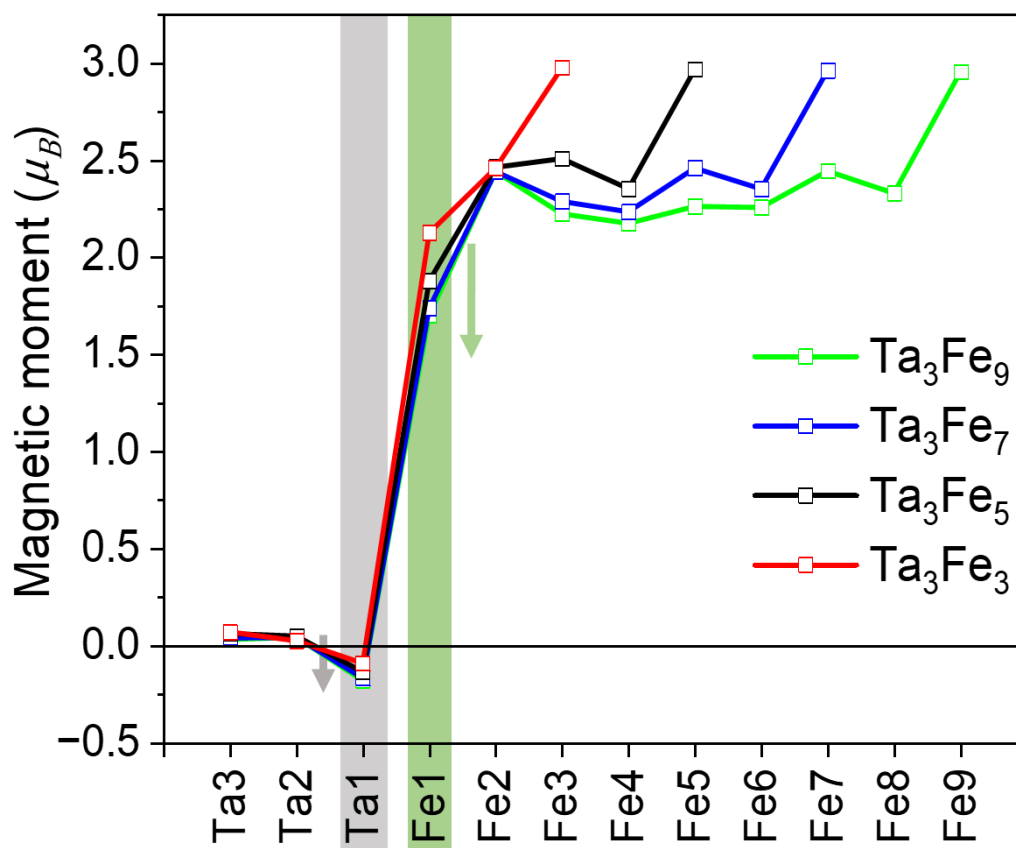


Figure S1 The magnetic moment per atom calculated for different Fe thicknesses in Ta/Fe interface. The green (gray) arrow represents the reduction (increase) of the Fe1 (Ta1) moment with the increase of Fe thickness.

As discussed in the main text, the structural relaxation induced by increasing the Fe thickness has a direct impact on the magnetic properties of Ta/Fe interface. Figure S1 shows the magnetic moment per atom calculated for different Fe thicknesses. The interfacial Fe1 atom has a reduced magnetic moment as the Fe layer gets thicker; a reduction of about 20% is found between  $\text{Ta}_3\text{Fe}_3$  and  $\text{Ta}_3\text{Fe}_9$  structures. On the other hand, the magnetic moment of the interfacial Ta1 atom increases negatively. Those two behaviors are mediated by the change in the  $d$ -orbital occupations, which in turn originates from the decrease of the interfacial distance ‘ $z$ ’ as shown in Fig.4 of the main text. For instance, Figure S2 shows the projected density of states (PDOS) of the  $d_{z^2}$  and  $d_{xz}$  orbitals of the Ta1 atom compared for  $\text{Ta}_3\text{Fe}_3$  and  $\text{Ta}_3\text{Fe}_5$ . It can be seen that the splitting between the occupied majority and minority spin states increases leading to the increase of the overall magnetic moment of Ta1 with the Fe thickness. The occupied states below the Fermi energy ( $E_F$ ) are integrated to obtain the orbital occupation presented in the main text and used in the framework of the first-order perturbation theory analysis.

It is also important to point out that the Ta/Fe interface features a decrease of the interfacial Fe1 atom (observed for all Fe thicknesses considered) compared to its bulk value ( $2.2 \mu_B$ ). This is consistent with the experimental observation that FeCoB becomes paramagnetic when too thick unoxidized Ta is deposited atop (see Figure 2 and [23]). At the same time, a small negative magnetic moment is induced on the interfacial Ta1 atom.

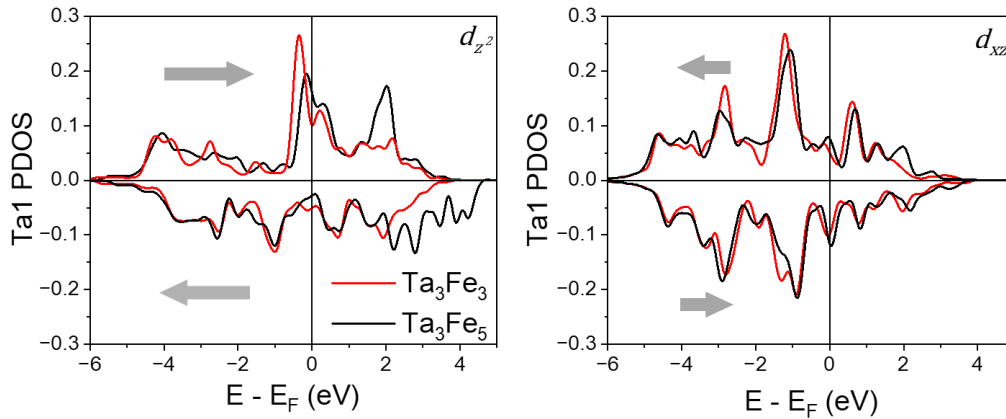


Figure S2 Projected density of states (PDOS) of the  $d_{z^2}$  and  $d_{xz}$  orbitals of the interfacial Ta1 atom compared for  $\text{Ta}_3\text{Fe}_3$  and  $\text{Ta}_3\text{Fe}_5$ . The occupied states below the Fermi energy ( $E_F$ ) are integrated to obtain the orbital occupation presented in the main text. The weights of the arrows designate the size of the shift of the occupied states when increasing the Fe thickness from  $\text{Ta}_3\text{Fe}_3$  to  $\text{Ta}_3\text{Fe}_5$ . Positive (negative) Ta1PDOS correspond to majority (minority) spins, respectively.

## 2. DMI variation with Ta oxidation and Fe thickness in Ta/Fe interface

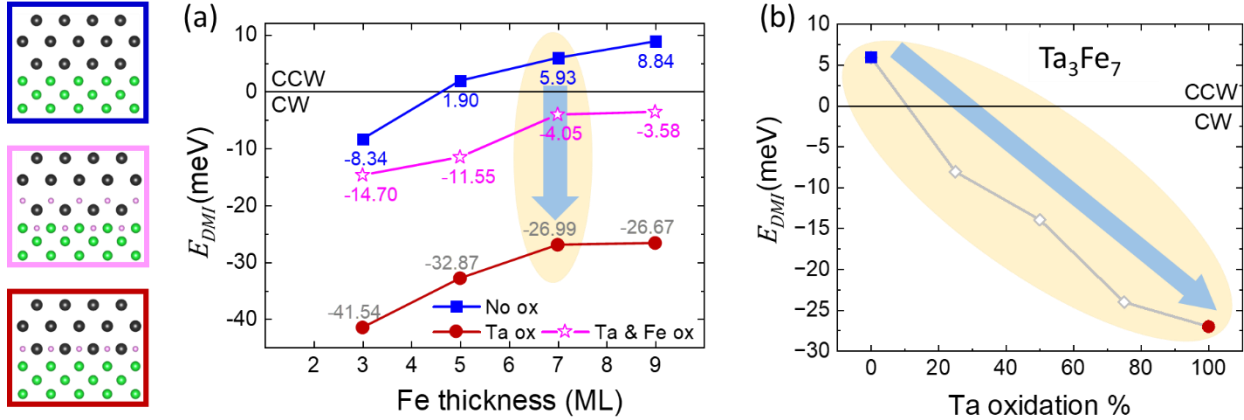


Figure S3 (Left) The crystallographic structures used for the three extreme cases considered for the DMI calculation are shown for non-oxidized Ta, fully oxidized Ta, and simultaneously oxidized Ta and Fe interface. (a) The DMI energy variation with the Fe thickness for different oxidation states of Ta/Fe interface. (b) The DMI energy variation as a function of the Ta oxidation percentage for a particular Fe thickness of seven monolayers. These data are summarized in Figure 3 of the main text.

Here, we present the detailed results of the DMI calculations. Figure S3(a) shows the variation of the DMI energy as function of the Fe thickness in  $Ta_3Fe_x$  interface calculated for different Ta oxidation states. First in the absence of oxygen, the square blue line shows that the DMI changes sign between three and five Fe monolayers. In the second extreme case where the Ta interfacial layer is fully oxidized, the DMI preserves its negative sign but decreases in value for thicker Fe. The case of overoxidation is modelled by fully oxidizing both the interfacial Fe and Ta layers (magenta stars in Figure S3(a)). Interestingly, the oxidation of the Fe layer decreases the DMI values compared to the case where only Ta is oxidized. To demonstrate the DMI dependence on the Ta oxidation, we plot in Figure S3(b) the variation of the DMI energy as function of the oxygen percentage of the Ta interfacial layer for the particular seven monolayer Fe thick system  $Ta_3Fe_7$ . The DMI changes sign at low oxidation percentages (below 25%) beyond which its value increases with the increase of the oxygen percentage. The full map of the DMI energy varying with both Ta oxidation percentage and the Fe thickness is presented in Figure 3 of the main text.



### 3. Interlayer and intralayer contributions of DMI

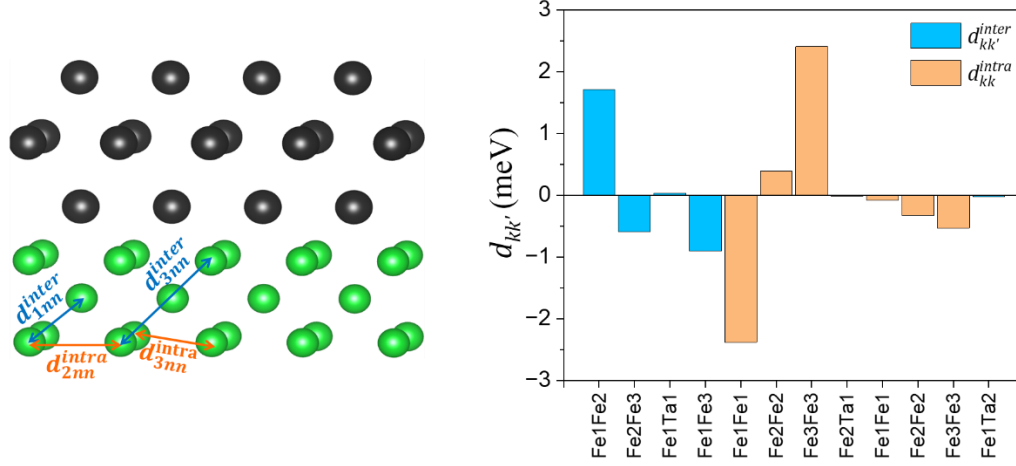


Figure S4 The intra- and interlayer DMI interactions up to the third nearest neighbor are represented on the crystal structure of Ta/Fe system. The calculated layer-resolved intra- and interlayer contributions to the DMI energy are represented by orange and blue bars, respectively.

The DMI energy in a bcc structure can be splitted into two contributions, interlayer  $E_{DMI}^{inter}$  and intralayer  $E_{DMI}^{intra}$ . Considering up to third nearest neighbor, we find:

$$E_{DMI}^{inter} = 8\sqrt{2} \sin \theta d_{1nn}^{inter} + 8\sqrt{2} d_{3nn}^{inter}, \text{ and}$$

$$E_{DMI}^{intra} = 8 d_{2nn}^{intra} + 8\sqrt{2} d_{3nn}^{intra},$$

where  $d$  is the microscopic DMI coefficient describing the interaction between two neighboring atoms as represented on the crystal structure in Figure S4(left).  $\theta$  designates the angle between the unit vector connecting the two nearest neighbors atoms in the adjacent planes and the normal to the surface.

To calculate the layer resolved DMI  $E_k^{intra}$  of atomic layer  $k$  from first-principles, we construct a spin spiral in this layer and fix the spins of the other layers in the  $y$ -crystallographic direction. Besides,  $E_{k,k'}^{inter}$  is calculated by constructing two spirals in the bi-layers  $k$  and  $k'$ . The results of those series of calculations for Ta<sub>3</sub>Fe<sub>3</sub> structure are presented in Figure S4. It can be seen that the largest intralayer DMI contributions are the interfacial Fe1  $E_{Fe1}^{intra}$  and the vacuum interface Fe3 showing opposite signs. On the other hand, the large interlayer DMI  $E_{Fe1,Fe2}^{inter}$  is compensated by the opposite sign of  $E_{Fe1,Fe3}^{inter}$  together with  $E_{Fe2,Fe3}^{inter}$ . In an overall picture, the summation of the layer resolved DMI energy comprising both intra- and interlayer contributions  $\sum_k E_k^{intra} + \sum_{k,k'} E_{k,k'}^{inter} = -7.84$  meV is within a margin of 6% difference from the calculated total DMI energy  $-8.34$  meV. This slight difference, which demonstrates the accuracy of our results, is attributed to the fact that calculations with different constrained configurations cannot be strictly equivalent.

#### 4. Effect of Ta thickness on DMI

In the following, we justify choosing three layer thick Ta layer in the calculations. Figure S5 compares the DMI energy calculated for  $\text{Ta}_3\text{Fe}_7$  and  $\text{Ta}_5\text{Fe}_7$  for both the non-oxidized and oxidized cases. It shows that increasing the Ta thickness does not influence the DMI sign while it has minor effect on the DMI value. Thus, we believe that this will not affect the main trends and conclusions drawn in this work.

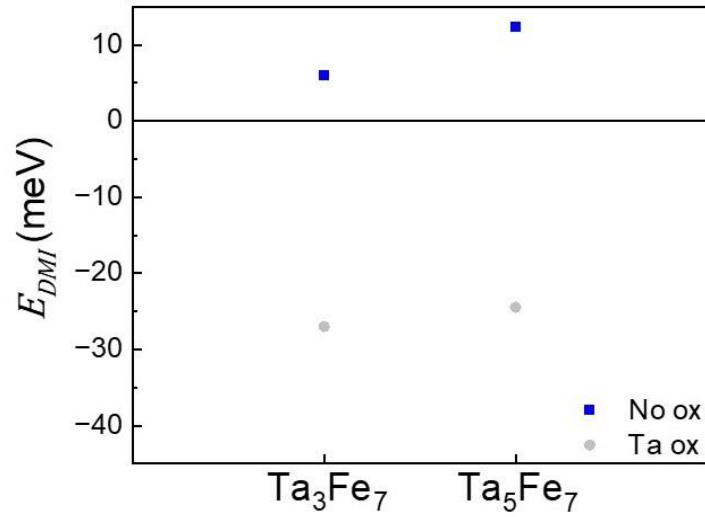


Figure S5 DMI energy for two Ta thicknesses, both in the oxidized and not oxidized cases.

### 5. The effect of bulk and interface Ta-oxidation on the DMI

Here, we verify that to model the effect of Ta oxidation on the DMI in Ta/Fe oxidizing the interfacial layer Ta1 only is sufficient. We choose the  $\text{Ta}_5\text{Fe}_7$  system since it enables to track the DMI energy as the oxygen atom approaches from the vacuum interface towards the Fe interface (see crystal configurations in Figure S7). The calculations show that oxidizing the whole Ta layer yields a DMI energy very close to the case where only the interfacial Ta1 is oxidized (represented by gray star in Figure S6). Importantly, the DMI is not significantly affected unless the oxygen atom is placed three monolayers away from the Fe interface (Ta3-4-5 configuration). Beyond this, the DMI energy converges to values close to the non-oxidized case (shown by blue crossed triangle in Figure S6). For convenience, we show also on the bottom axis the distance between the interfacial Fe1 and the first oxygen atom ( $d_{\text{Fe-O}}$ ). Therefore, those results support what was previously mentioned about the decisive role of the interfacial Ta atom in the DMI trends and highlights once again the minor importance of the Ta thickness and the oxidation of the Ta layer at more than 3 monolayers from the interface.

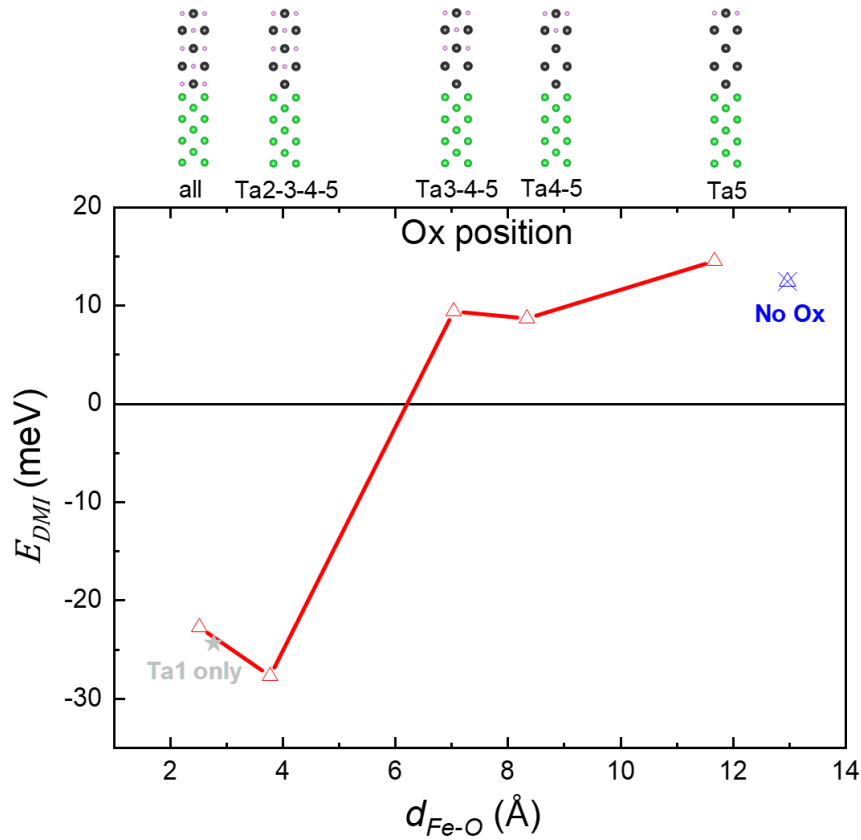


Figure S6 DMI energy in a Fe/TaOx stack with varying distance between the Fe and Oxygen in the Ta, as represented above the graph. The change of sign occurs when oxygen is more than 3 Ta layers apart. The oxidized and not oxidized interface cases used in the main text are represented with the grey star and blue crossed triangle respectively.